Unsteady standoff shock behaviour associated with supersonic impinging jets

T. H. New[1,*], H. D. Lim[2], R. Mariani[3], R. G. Y. You[1], W. L. Chan[1]

1: School of Mechanical and Aerospace Engineering, Nanyang Technological University, Singapore
2: School of Civil, Aerospace and Design Engineering, University of Bristol, United Kingdom
3: Department of Engineering Mechanics, KTH Royal Institute of Technology, Sweden
*Corresponding author: dthnew@ntu.edu.sg

Keywords: Standoff shock, shock unsteadiness, schlieren visualization, numerical simulation.

ABSTRACT

It was observed in an earlier study [Lim, H. D., New, T. H., Mariani, R., & Cui, Y. D. (2019). Effects of bevelled nozzles on standoff shocks in supersonic impinging jets. Aerospace Science and Technology, 94, 105371.] that standoff shocks in M=1.45 supersonic impinging jets produced by non-bevelled and bevelled nozzles under small separation distances may undergo large and abrupt fluctuations in their positions above the impingement points. This occurs when the separation distance is h/d=1.5 and for nozzle-pressure-ratio (NPR) between NPR=4 and 5, where h is the distance between the nozzle exit and flat-wall and d is the jet diameter. It has to be highlighted that the observed behaviour is unlike the more minor positional fluctuations typically associated with supersonic impinging jets. To reveal further details on the unsteadiness of the standoff shock, color schlieren results will be presented here to shed more light on the flow phenomenon, while initial modelling efforts to reproduce these standoff shock behaviour will be elaborated. Present results reinforce the notion that the large standoff shock fluctuations are due to the standoff shock trying to achieve pressure equilibrium through abrupt displacements when variation in the NPR changes the location of the shock reflection point. Considering the small separation distance used, small NPR changes are able to trigger abrupt standoff shock unsteadiness.

1. Introduction

Supersonic impinging jets have been extensively studied over the past decades through experimental and numerical means, where much emphasis have been placed upon the resulting shock behaviour and acoustic emissions. There are strong interests with regards to their fundamental flow behaviour and associated efficacy when their operating conditions vary, as that could lead to more optimised outcomes when they are utilised in high-speed engineering applications, such as cold-spraying, launch platforms, as well as heat and mass transfer applications. Some of the key operating conditions that could be varied would include nozzle-pressure-ratio (NPR), nozzle exit-to-wall separation distance and jet exit Mach number. While supersonic jets can be set to impinge upon a wide range of surface types, the present study will focus on flat-wall impingements.

For flat-wall impingements, it is very common to see dimensionless separation distances of h/d=2 (where h is the distance between jet exit and flat wall and d is the jet diameter) and beyond being studied and analysed in great details and effects, for instance, by Dauptain et al. (2012); Yao et al. (2012); Mason-Smith et al. (2015); Wilke & Sesterhenn (2017); Karami et al. (2020); Karami & Soria (2021); Cui et al. (2021); Sikroria et al. (2022); Li et al. (2023). In contrast, flat-wall impingements making use of separation distances smaller than h/d=2 are not as well-studied, other than a few exceptions such as Henderson (2002); Henderson et al. (2005); Lim et al. (2019); Nguyen et al. (2020). In particular, Lim et al. (2019) paid special attention towards the use of separation distances that ranges from h/d=1 to 2 and how it affects the formation and stability of the resulting standoff shock. It is worthwhile to highlight that Lim et al. (2019) had observed two different types of standoff shock unsteadiness during their testing. First, the more typical minor fluctuations or "jitters" in the standoff shock location above the impingement point, which have also been observed in and documented by Cui et al. (2021) recently. Second, they also observed occurrences of much larger abrupt "jumps" in the standoff shock location associated with interactions between the shock reflection point and standoff shock. These interactions would lead to new pressure equilibrium conditions, which in turn would cause an abrupt change in the standoff shock location.

For cold-spraying, uniformity and consistency of the remanufactured surface needs to be maintained at high levels to ensure overall structural integrity, especially if the remanufactured component were to be used in critical applications involving harsh environments, such as compressor or turbine blades in turbofan engines. Minimising jet shear layer thickness such that a jet impingement area that maximises the supersonic jet core coverage is usually desirable to achieve high uniformity and consistency levels. One of the more intuitive ways to accomplish that could involve positioning the nozzle closer to the surfaces to be cold-sprayed, meaning adopting shorter than usual separation distances. While minor standoff shock fluctuations should not affect the remanufactured surface uniformity and consistency that much, the same may not be assumed if the standoff shock were to undergo large-scale abrupt positional variations such as those observed by Lim et al. (2019). To investigate further, the present study follows up upon that earlier study by analysing new colour-schlieren results captured through high-speed imaging devices, which made it easier to identify additional compressible flow/shock features than conventional schlieren approaches and could shed more light upon the large scale positional fluctuations. In addition, complementary efforts were made along the numerical front to model supersonic impinging jets under the same conditions used during the experiments to clarify certain aspects of the experimental observations that might have been more ambiguous due to the more qualitative nature of the schlieren imaging approach. In particular, future plans are to model the abrupt standoff shock jumps when the NPR varies during the jet impingement experiments conducted by Lim et al. (2019). Doing so would offer access to the flow properties associated with the standoff shock's large scale position fluctuations and their influence on the wall pressure fluctuations, which are of significant and practical interest for cold spray applications.

2. Experimental and Numerical Procedures

2.1. Experimental setup and technique

All supersonic jets used in the experiments were produced by a compressed air based blow-down facility where the resulting supersonic jets were exhausted into a temperature and humidity controlled laboratory environment. The compressed air came from two air tanks that could store up to 69 bar stagnation pressure, which was then directed through a series of flow control valves and regulators before it entered the settling chamber of the supersonic jet apparatus. Subsequently, it would pass through a series of flow straighteners and conditioning devices, before entering a convergent-divergent section to produce supersonic jets that exhausted from a nozzle with a design Mach number of M=1.45. The supersonic jet was exhausted at underexpanded conditions of NPR=4 and 5, depending on the test conditions. The nozzle has a inner diameter of 12.7mm and lip thickness of 0.5mm. Finally, a rigid 6mm thick, $30d \times 30d$ square flat plate was used as the impingement surface and located at h/d=1 and 1.5 away from the nozzle exit.

For schlieren imaging, a modified, single-pass Z-type mirror schlieren setup was used. Broadband illumination was provided by a 200W white LED light source, while two 300mm diameter parabolic mirrors with 3m focal lengths directed the light into the test-section and onto the knife-edge. The latter was oriented normal to the supersonic jet flows to highlight the shock structures. An IDT NX4-S1 grayscale camera with a Nikon AF Micro-Nikkor 200mm f/4D IF-ED lens was then used to image the schlieren visualizations at 1000 frames-per-second. As the present emphasis is on the standoff shock structures, an relatively moderate exposure time of 200μs was used to reduce flow turbulence effects. As for colour schlieren experiments, they were produced via a 6mm strip rainbow filter oriented parallel to the direction of the impingement surface. All colour schlieren images were captured using a Nikon D7200 digital single-reflex (DSLR) camera with image resolution of 6000px by 4000px, where the camera shutter time was set to 1/8000 at ISO1000 sensitivity. Images were then focused directly on the CCD screen of the camera using three macro lenses with magnifying factors of +1, +2, and +4, with the lens with the largest magnifying factor set closest to the camera. More details can be found in Mariani et al. (2020).

2.2. Numerical setup and technique

To complement the supersonic impinging jet experiments, OpenFOAM software (ESI-OpenCFD, 2021) was utilised together with *rhoCentralFoam* compressible flow solver and Large Eddy Simulation turbulence formulations, which had been used successfully by Cui et al. (2021); Zang et al. (2018) and is hence well-established in the modelling of supersonic jet-based flow scenarios. The objective is to model the experimental scenario to replicate both the minor and abrupt changes in the standoff shock behaviour. To simplify the flow configuration, the supersonic jet was modelled based on an nozzle exit mach number of M=1.45 and NPR=4 according to the conditions used in Lim et al. (2019). A three-dimensional, axisymmetric computational domain was used, where the

radial extent is $10d$ with the supersonic jet exit located at h/d=1.5 above and discharging vertically downwards onto a no-slip circular wall/boundary. A fully structured mesh with an O-H grid topology for the mesh core was used, with graded grid spacing such that the mesh resolution was higher along the impinging wall, nozzle lip, and in the expected shear layer regions. To minimise any boundary effects, the flow around the jet nozzle was also modelled up to $3d$ upstream of the nozzle exit.

All outlet boundary surfaces were set to *waveTransmissive* boundary condition to allow flow pass-through and avoid any pressure wave reflections from occurring. Additionally, the internal domain where the supersonic jet was issued into was initialised with standard atmospheric pressure, 300K total temperature, and zero velocity throughout at the beginning of the numerical simulations. Based on these initial conditions, the supersonic jet would exhaust initially as a starting jet before settling down to a quasi-steady supersonic impinging jet. A second-order Crank–Nicholson approach was adopted to ensure temporal accuracy, coupled with time-stepping to maintain a stable numerical scheme with a Courant number of below 0.3. Finally, a mesh convergence check was conducted based on three different mesh configurations comprising of 8.5 million, 17.7 million and 41 million. The mesh convergence check reveals that the medium mesh is adequate to capture the intricate formations and interactions between the compressible jet shear layer vortices and standoff shock, which can lead to the unsteadiness observed in the latter. Hence, the medium mesh was selected as the configuration of choice for subsequent analyses.

3. Results and Discussion

3.1. Experimental results

Figure 1 shows the colour schlieren images captured for underexpanded jets, at the same NPR and separation distance, where two views along the peak-to-peak and trough-to-trough planes for non-axisymmetric nozzles are presented. The geometry and position of the standoff shocks are relatively similar across the different test cases, despite an earlier study showing geometrical modifications to the nozzle exit are effective at controlling the spread rate of underexpanded round jets (Wu et al., 2019). This can be attributed to the relatively significant distance between the reflection point (defined as the confluence of the intercepting oblique shocks and reflected shocks following the definition of Lim et al. (2019)) and the standoff shock, which corroborates well with the study by Lim et al. (2019).

In the region just above the impingement surface, there is a unique flow feature that is most noticeably different for the notched nozzle as shown in Figure 1(d,e). This flow feature has strong variations in the vertical density gradients of the flow (i.e., the knife-edge orientation was horizontal), which suggests that the use of nozzle modifications as a passive flow control method would lead to a highly localised high pressure region on the impingement plate. Cui et al. (2021) observed a similar feature in their starting supersonic impinging jet simulations, indicating that this

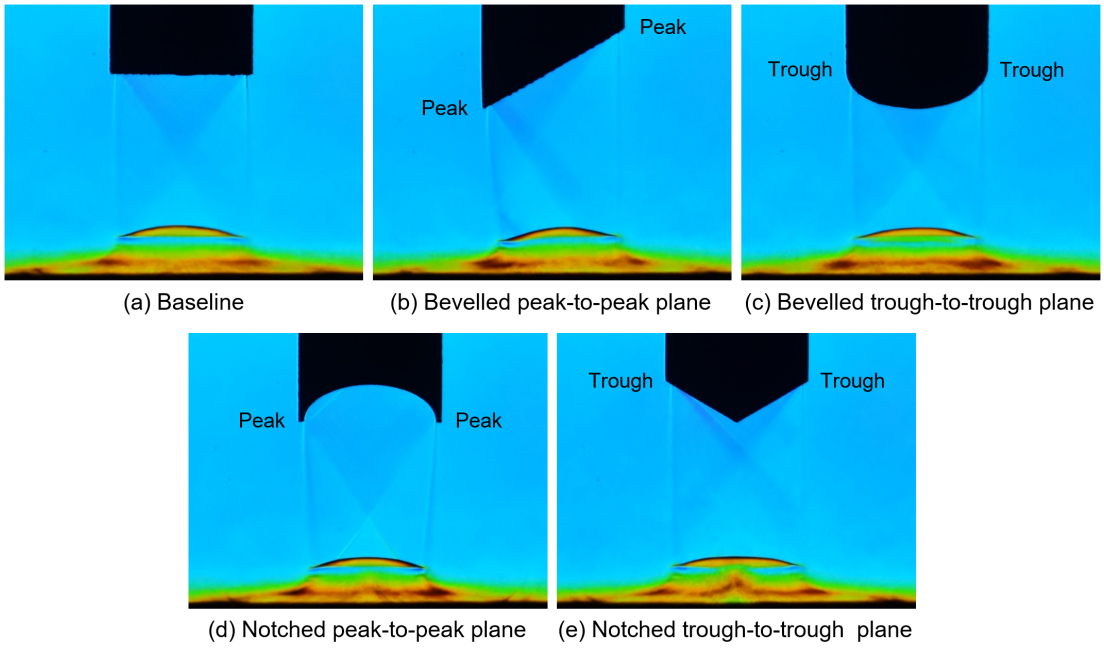

Figure 1. Color schlieren images captured for all test nozzles at NPR=4 and h/d=1.5 separation distance.

phenomenon is not unique to just pseudo-steady impinging jet scenarios but transient ones as well. As it was not possible to capture global transient pressure distributions during the experimental stage, numerical simulations will be used to investigate them further.

In particular, the sensitivity of the standoff shock to the reflection point location can be seen in Figure 2, which shows a sequence of schlieren images for the underexpanded baseline nozzle as the NPR increases gradually from 4.5 to 5.0. During this process, the distance between the reflection point to the standoff shock reduces gradually, until the reflection point reaches the standoff shock with the latter incurring an abrupt upstream jump in its location. This distance is clearly a key parameter that has a strong influence on the geometry, position and stability of the standoff shock. The reflection of pressure waves off the impingement surface is another factor that can influence the standoff shock. As can be seen in the recent study by Cui et al. (2021), there exists complex interactions of pressure waves within the recirculating region below the standoff shock. However, it should also be noted that the jet Mach number and separation distance were different from that used here. Similar increments in the NPR were used on the bevelled nozzle and the outcomes are presented in Figure 3. Similar to the previous baseline nozzle, the standoff shock moves gradually closer to the reflection point as the NPR increases until it reaches a crucial point where it begins to oscillate rapidly as shown in Figure 3(e, f). In fact, the oscillation frequency is so high that the frame-rate of high-speed camera was insufficient to capture the oscillating standoff shock clearly at that point. Similar to the global transient pressure distributions, numerical simulations will be used to capture the details of these small- and large-scale shock unsteadiness. The next section will describe the initial simulation results obtained thus far.

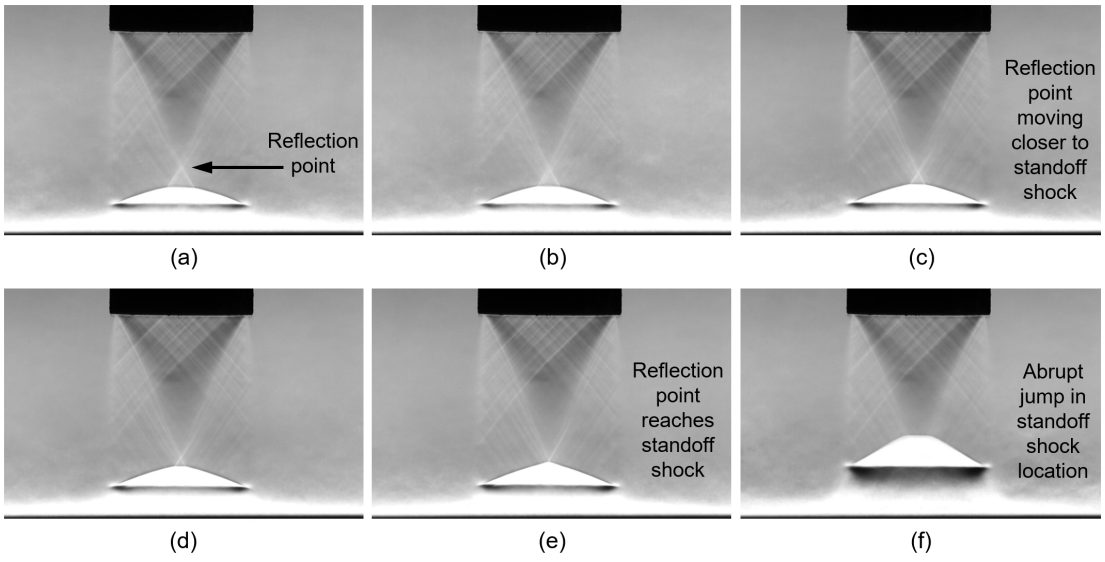

Figure 2. Grayscale schlieren images captured for baseline nozzle as NPR increases from 4.5 to 5 gradually. Note the abrupt jump in standoff shock height from (e) to (f). Images are overexposed to highlight the standoff shock geometry.

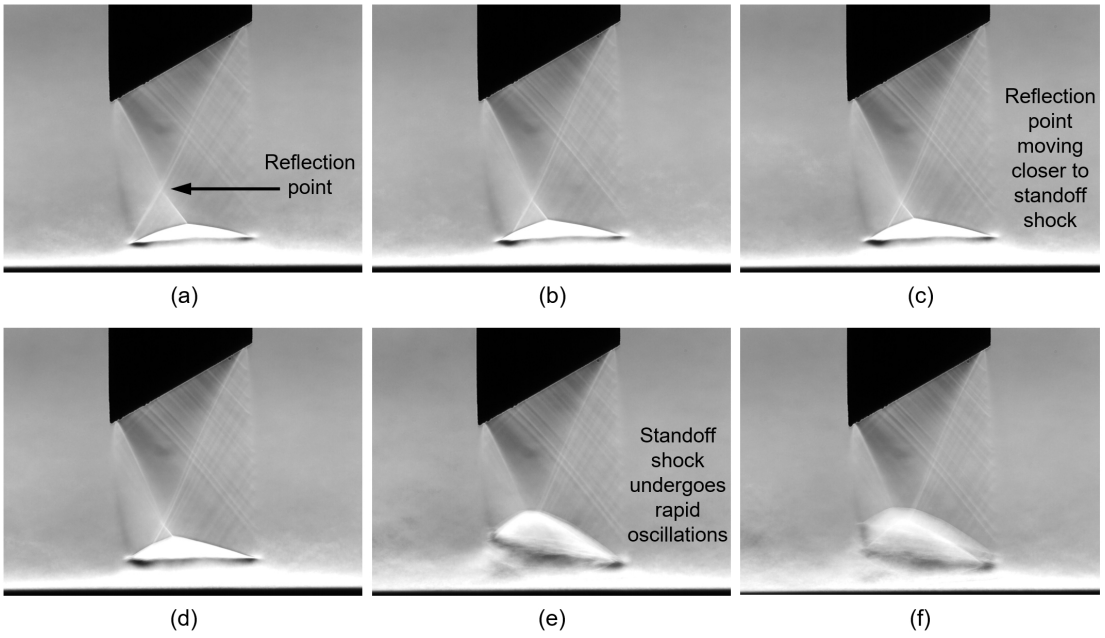

Figure 3. Grayscale schlieren images captured for bevelled nozzle as NPR increases from 4.5 to 5 gradually. Note the abrupt oscillations in standoff shock height in (e) and (f). Images are again overexposed to highlight the standoff shock geometry.

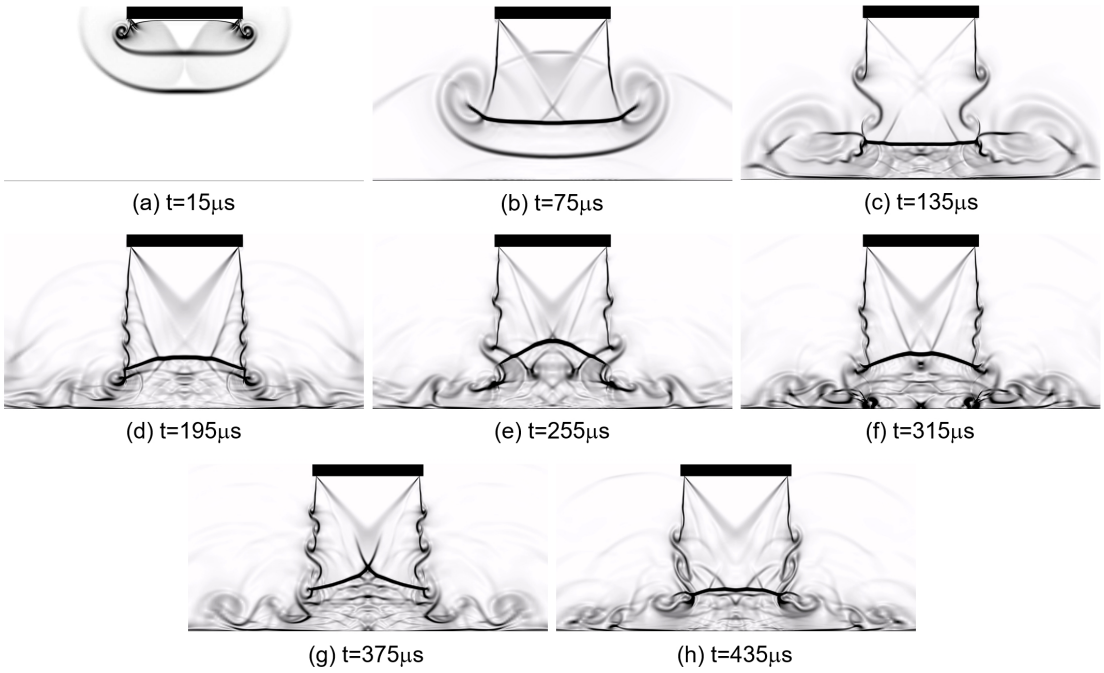

Figure 4. Instantaneous numerical schlieren results captured for the starting supersonic jet issuing from the baseline nozzle.

3.2. OpenFOAM numerical results

Figure 4 shows some early results from the OpenFOAM simulations, where instantaneous numerical schlieren results associated with the M=1.45 supersonic jet exhausting from the baseline nozzle and subsequently impinging upon the flat-wall located at h/d=1.5 away are presented. It can be readily appreciated from Figure 4(a,b) that the supersonic starting jet flow produces a bow shock ahead of the starting vortex-ring structure in the initial stages before they encounter the flat-wall. Once they impinge upon the flat-wall, the starting vortex-ring structure increases in diameter and spreads radially away from the centerline. At the same time, the bow shock reflects off the flat-wall and travels upstream towards the nozzle. Once the reflected bow shock encounters the nozzle exit wall, it triggers the formation of regular shear layer instabilities that convect towards and interact with the standoff shock "tails" along the jet shear layer, as shown in Figure 4(c). The impinging jet flow will gradually settle into a quasi-steady condition as seen in Figure 4(d-f), though it remains clear that the standoff shock continues to undergo significant unsteadiness in its physical location and profile. Note that these fluctuations are relatively minor and expected to settle into those observed by Cui et al. (2021) earlier. Next, Figure 5 shows the corresponding Mach number distributions corresponding to the timings in Figure 4, where the impact on the recirculating low-speed region just above the flat-wall due to the fluctuating standoff shock is more apparent. Additionally, it can be clearly discerned that the compressible shear layer vortices remain relatively coherent after they are redirected to flow radially away along the flat-wall. These results resemble closely to earlier supersonic jet impingement studies and provide confidence for future simulations.

Last but not least, Figure 6 shows the transient pressure fluctuations both in terms of peak pres-

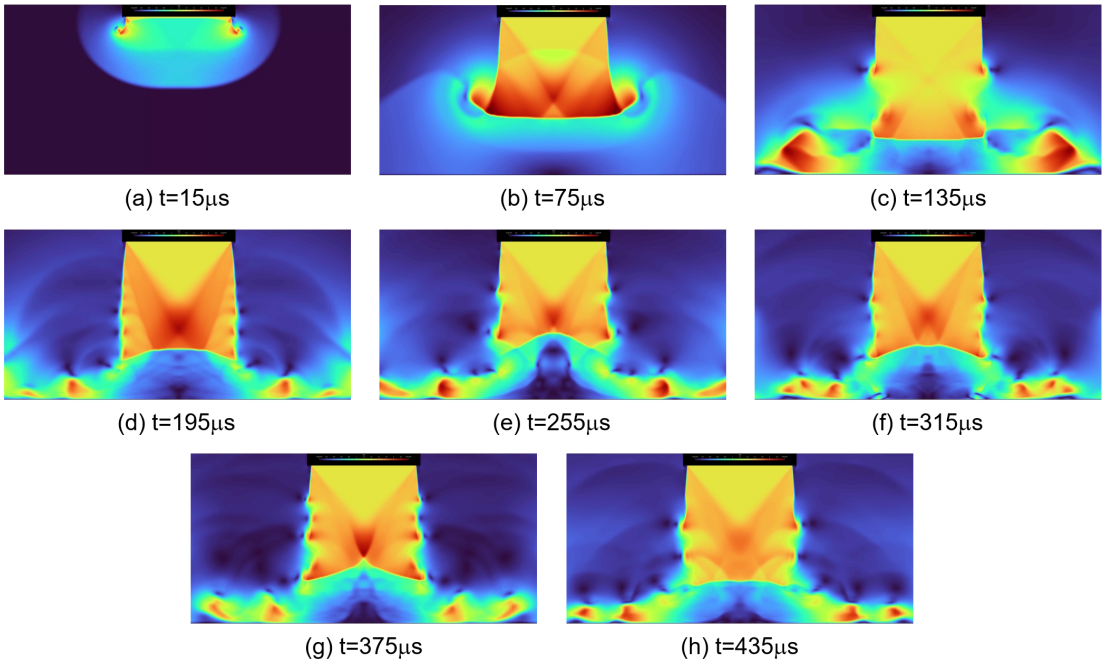

Figure 5. Instantaneous Mach number distributions for the starting supersonic jet issuing from the baseline nozzle.

sure levels and radial extents along the impingement surface from $t = 135\mu s$ onwards (i.e., same time corresponding to Figure 4(c)), since the jet has not encountered the flat-wall at $t = 15\mu s$ and $75\mu s$. Pressure distributions can be observed to fluctuate significantly across the plots in the figure. However, these pressure fluctuations are within expectations due to the significant variations in the standoff shock and recirculating region behaviour seen in Figures 4 and 5 previously. More importantly, the preceding results show that the present numerical approaches are able to resolve the standoff shock and its fluctuations reasonably well and future work would include NPR variations from NPR=4 to 5 to replicate the large-scale abrupt standoff shock oscillations.

4. Conclusions

Conventional and color schlieren imaging techniques were used to investigate further small-scale fluctuations in the standoff shock position produced by a M=1.45, NPR=4 supersonic jet impinging upon a flat wall with a separation distance of h/d=1.5. Such fluctuations are in-line with observations made by earlier studies. On the other hand, when the NPR was increased gradually to NPR=5 while the supersonic jet continues to impinge upon the surface, the standoff shock will undergo an abrupt upstream jump in its position and profile. This is deduced to result from the downstream shift in the shock reflection point location as the NPR increases, where the abrupt jump will occur once the shock reflection point coincides with the standoff shock. OpenFOAM-based numerical simulations were also being conducted to complement the present supersonic impinging jet experiments, from the starting stage to the quasi-steady stage. Initial results clarify the formation and unsteadiness of the standoff shock in the early stages and how the surface pressure distributions

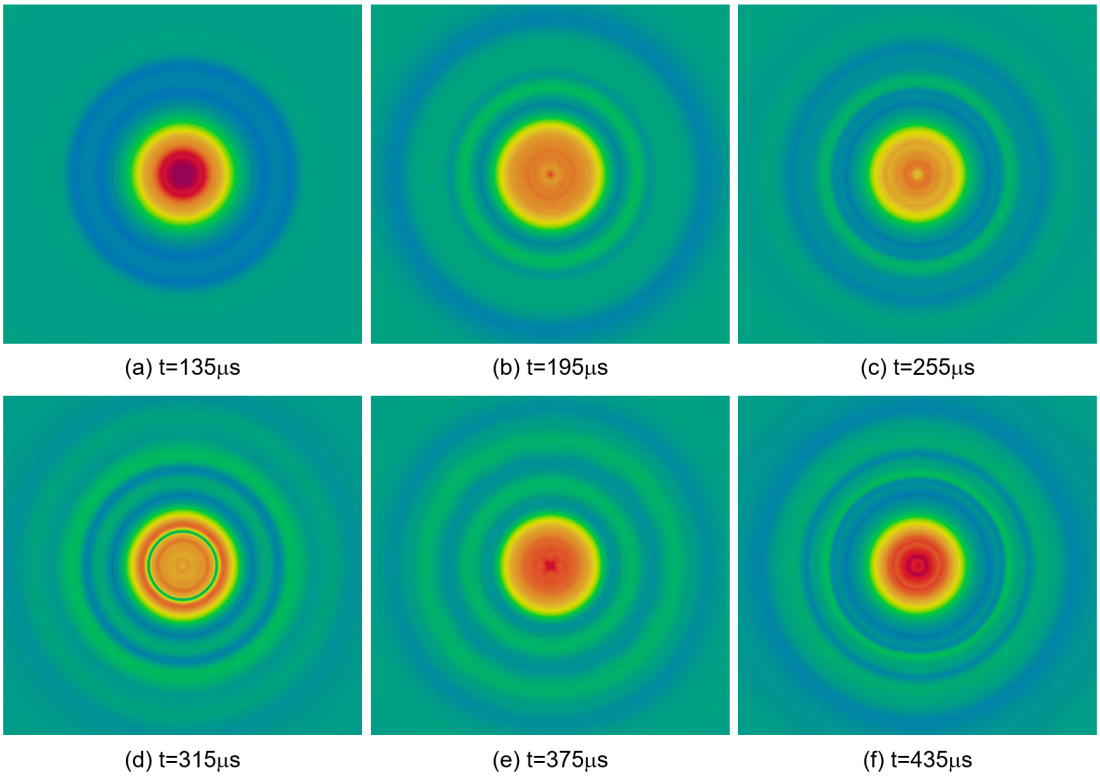

Figure 6. Instantaneous wall pressure fluctuations for the starting supersonic jet issuing from the baseline nozzle.

are affected. It is expected that the availability of their outcomes will aid further clarifications upon the abrupt jumps in the standoff shock in the future.

Acknowledgements

The authors gratefully acknowledge the support provided by the Nanyang President Graduate Scholarship for the second author during his PhD candidature at Nanyang Technological University, Singapore, while working on the project. Support from Singapore Ministry of Education Tier-2 AcRF and Tier-1 AcRF (grant numbers MOE2014-T2-1-002 and RG67/22) for the third and fourth authors, respectively, are appreciated as well. Lastly, the computational work for this article was fully performed on resources of the National Supercomputing Centre, Singapore (`https://www.nscc.sg`).

Nomenclature

NPR	Nozzle pressure ratio
M	Mach number
d	Jet diameter [mm]
h	Separation distance from jet exit to flat wall [mm]

t Time [μs]

References

Cui, W., Xu, J., Wang, B.-C., Zhang, P., & Qin, Q. (2021). The initial flow structures and oscillations of an underexpanded impinging jet. *Aerospace Science and Technology*, *115*, 106740.

Dauptain, A., Gicquel, L. Y. M., & Moreau, S. (2012). Large eddy simulation of supersonic impinging jets. *AIAA Journal*, *50*(7), 1560–1574.

ESI-OpenCFD. (2021). *OpenCFD release OpenFOAM®v2112.* (`https://www.openfoam.com/news/main-news/openfoam-v2112`, Last accessed: Dec 27 2023)

Henderson, B. (2002). The connection between sound production and jet structure of the supersonic impinging jet. *The Journal of the Acoustical Society of America*, *111*(2), 735–747.

Henderson, B., Bridges, J., & Wernet, M. (2005). An experimental study of the oscillatory flow structure of tone-producing supersonic impinging jets. *Journal of Fluid Mechanics*, *542*, 115–137.

Karami, S., Edgington-Mitchell, D., Theofilis, V., & Soria, J. (2020). Characteristics of acoustic and hydrodynamic waves in under-expanded supersonic impinging jets. *Journal of Fluid Mechanics*, *905*, A34.

Karami, S., & Soria, J. (2021). Influence of nozzle external geometry on wavepackets in underexpanded supersonic impinging jets. *Journal of Fluid Mechanics*, *929*, A20.

Li, X., Wu, X., Liu, L., Zhang, X., Hao, P., & He, F. (2023). Acoustic resonance mechanism for axisymmetric screech modes of underexpanded jets impinging on an inclined plate. *Journal of Fluid Mechanics*, *956*, A2.

Lim, H. D., New, T. H., Mariani, R., & Cui, Y. D. (2019). Effects of bevelled nozzles on standoff shocks in supersonic impinging jets. *Aerospace Science and Technology*, *94*, 105371.

Mariani, R., Lim, H. D., Zang, B., Vevek, U. S., New, T. H., & Cui, Y. D. (2020). On the application of non-standard rainbow schlieren technique upon supersonic jets. *Journal of Visualization*, *23*, 383–393.

Mason-Smith, N., Edgington-Mitchell, D., Buchmann, N. A., Honnery, D. R., & Soria, J. (2015). Shock structures and instabilities formed in an underexpanded jet impinging on to cylindrical sections. *Shock Waves*, *25*, 611–622.

Nguyen, T., Maher, B., & Hassan, Y. (2020). Flowfield characteristics of a supersonic jet impinging on an inclined surface. *AIAA Journal*, *58*(3), 1240–1254.

Sikroria, T., Sandberg, R., Ooi, A., Karami, S., & Soria, J. (2022). Investigating shear-layer instabilities in supersonic impinging jets using dual-time particle image velocimetry. *AIAA Journal*, *60*(6), 3749–3759.

Wilke, R., & Sesterhenn, J. (2017). Statistics of fully turbulent impinging jets. *Journal of Fluid Mechanics*, *825*, 795–824.

Wu, J., Lim, H. D., Wei, X., New, T. H., & Cui, Y. D. (2019). Flow characterization of supersonic jets issuing from double-beveled nozzles. *Journal of Fluids Engineering*, *141*(1), 011202.

Yao, Z., Liu, H., & Zhang, X. (2012). Interaction of shocks and vortices in a highly underexpanded supersonic impinging jet. *AIAA Journal*, *50*(5), 1169–1176.

Zang, B., Vevek, U. S., Lim, H. D., Wei, X., & New, T. H. (2018). An assessment of OpenFOAM solver on RANS simulations of round supersonic free jets. *Journal of Computational Science*, *28*, 18–31.